Available online at www.sciencedirect.com

ScienceDirect

Energy Procedia 50 (2014) 87 – 96

Energy Procedia

The International Conference on Technologies and Materials for Renewable Energy, Environment and Sustainability, TMREES14

The influence of Zr/Ti content on the morphotropic phase boundary and on the properties of PZT–SFN piezoelectric ceramics

Fares Kahoul [a,b], Louanes Hamzioui [a,b], Ahmed Boutarfaia [a,b,*]

[a] *Université Kasdi Merbah Ouargla, laboratoire de génie des procédés, Faculté des sciences appliquées, Ouargla 30000 Algérie*
[b] *Département de chimie, laboratoire de chimie appliquée, Université de Biskra B. P. 145, RP-Biskra 07000, Algérie*

Abstract

The polycrystalline samples of (1-x)Pb $(Zr_y\ Ti_{1-y})O_3$-xSm$(Fe^{3+}_{0.5},\ Nb^{5+}_{0.5})O_3$ [PZT–SFN] (where x = 0.02 and $0.41 \leq y \leq 0.57$) were prepared by a high-temperature solid-state reaction technique. All samples were sintered at a temperature of 1150 ^{0}C for 2 h. The crystallographic phase and microstructure of the ceramics were examined by using X-ray diffraction (XRD) and atomic force microscopy (AFM). The experimental result shows that the samples consist of a mixture of tetragonal and rhombohedral phases (morphotropic phase boundary MPB) in the range of $0.53 \leq y \leq 0.55$, grains grow up homogeneously and the minimum value of Curie temperature was obtained with y = 0.53 and 0.55. Main piezoelectric parameters are optimized at around y = 0.53 - 0.55 with a high piezoelectric coefficient (d_{31} = 106- 117 pC/N), a planar electromechanical coefficient (k_p = 61.7- 61.8 %), a high dielectric constant (ε_r = 798- 974) and a low dissipation factor (tan δ = 1.405% - 1.356%) measured at 1 kHz room temperature, which indicates that the PZT–SFN ceramics are promising for practical applications.

Selection and peer-review under responsibility of the Euro-Mediterranean Institute for Sustainable Development (EUMISD)

Keywords: Dielectric properties; Piezoelectric properties; PZT; XRD; Perovskite

1. Introduction

Lead-based perovskite ferroelectric ceramics are widely applied in multilayer capacitors, micro-electro

* Corresponding author. Tel.: +213 29 717 070; fax: +213 29 715 161.
E-mail address: Fares_260@yahoo.fr, Aboutarfaia@yahoo.fr

Selection and peer-review under responsibility of the Euro-Mediterranean Institute for Sustainable Development (EUMISD)
doi:10.1016/j.egypro.2014.06.011

mechanical systems (MEMS) and integrated devices such as ferroelectric memories, infrared sensors, micro actuators, etc.[1–5]. Many of these applications demand materials with excellent dielectric and ferroelectric properties. Lead zirconium titanate (PZT) is one of the best lead-based materials that have been studied extensively since late 1940s [6,7]. The dielectric characteristics of PZT ceramic changes with its stoichiometry [8]. PZT is an ABO_3 type perovskite structured material with A-site (Pb^{2+}) occupying the cubo-octohedral interstices described by the BO_6 site octahedral and has tetragonal, rhombohedral and orthorhombic phases at room temperature, depending on the value of Zr/Ti ratio. It has two morphotropic boundaries (MPB) at 53 / 47 Zr/Ti ratio, where it undergo phase transition from orthorhombic to low temperature rhombohedral and high temperature rhombohedral to tetragonal phases, respectively. All these compositions show cubic phase above transition temperature. The composition near MPB region normally show an increased capability of polarization and electromechanical response, which make them suitable for non-volatile memories and piezoelectric actuators [9–11]. PZT compositions show significant merit, when they are doped with foreign ions. Its dielectric and piezoelectric properties change, depending on the site occupied by the foreign ion in ABO_3 perovskite structure. Dopents are classified as isovalent, acceptors or donors [12]. Donors (trivalent ion at A site and pentavalent ion at B site) reduces the concentration of intrinsic oxygen vacancy created due to PbO evaporation and compensate the hole formed due to lead vacancies, which in tern increases bulk resistance of sample. Acceptors (monovalent at A site and trivalent at B site) introduces oxygen vacancies to maintain charge neutrality, due to this oxygen vacancy domain walls gets pinned and space charges are introduces, which in tern reduces grain resistance and inhibits domain motion [13], also acceptor-doped PZT shows poor hysteresis loop and low dielectric constant. Isovalent (divalent at A site and tetravalent at B site) doping tends to reduce the Curie temperature [9] and increases the density of PZT ceramic, which in tern effect the electrical properties.

The aim of the present study was, first, to carry out a structural study in a solid solution of PZT and SFN using X-ray diffraction. The system chosen for investigation is (1-x)Pb $(Zr_y\ Ti_{1-y})O_3$-xSm$(Fe^{3+}_{0.5},\ Nb^{5+}_{0.5})O_3$. A detailed systematic structural analysis was carried out for x = 0.02 compositions by varying the value of y. In this paper, an effort has been made to determine the MPB phase contents and study the changes in the phase fraction of these phases with variations in the Zr/Ti ratio. This will help to better determine how variations in the phase content affect local atomic arrangements and hence the properties; and, second, to efficiently combine the dielectric and electromechanical properties of this system. The relationship between electrical properties, microstructures and crystal structure are reported and discussed. The general chemical formula and compositions synthesized have been presented in Table 1.

Table 1. Stoichiometric compositions synthesized.

Composition Zr/Ti	Formula
41/59	$Pb_{0.98}Sm_{0.02}[(Zr_{0.41}Ti_{0.59})_{0.98}-(Fe^{3+}_{0.5}, Nb^{5+}_{0.5})_{0.02}]O_3$
43/57	$Pb_{0.98}Sm_{0.02}[(Zr_{0.43}Ti_{0.57})_{0.98}-(Fe^{3+}_{0.5}, Nb^{5+}_{0.5})_{0.02}]O_3$
45/55	$Pb_{0.98}Sm_{0.02}[(Zr_{0.45}Ti_{0.55})_{0.98}-(Fe^{3+}_{0.5}, Nb^{5+}_{0.5})_{0.02}]O_3$
47/53	$Pb_{0.98}Sm_{0.02}[(Zr_{0.47}Ti_{0.53})_{0.98}-(Fe^{3+}_{0.5}, Nb^{5+}_{0.5})_{0.02}]O_3$
49/51	$Pb_{0.98}Sm_{0.02}[(Zr_{0.49}Ti_{0.51})_{0.98}-(Fe^{3+}_{0.5}, Nb^{5+}_{0.5})_{0.02}]O_3$
51/49	$Pb_{0.98}Sm_{0.02}[(Zr_{0.51}Ti_{0.49})_{0.98}-(Fe^{3+}_{0.5}, Nb^{5+}_{0.5})_{0.02}]O_3$
53/47	$Pb_{0.98}Sm_{0.02}[(Zr_{0.53}Ti_{0.47})_{0.98}-(Fe^{3+}_{0.5}, Nb^{5+}_{0.5})_{0.02}]O_3$
55/45	$Pb_{0.98}Sm_{0.02}[(Zr_{0.55}Ti_{0.45})_{0.98}-(Fe^{3+}_{0.5}, Nb^{5+}_{0.5})_{0.02}]O_3$
57/43	$Pb_{0.98}Sm_{0.02}[(Zr_{0.57}Ti_{0.43})_{0.98}-(Fe^{3+}_{0.5}, Nb^{5+}_{0.5})_{0.02}]O_3$

2. Experimental procedures

Polycrystalline samples of a new materials of ceramics with general formula (1-x)Pb$(Zr_y\ Ti_{1-y})O_3$-xSm$(Fe^{3+}_{0.5}$, $Nb^{5+}_{0.5})O_3$ [while varying y (41% ≤ y ≤ 57% with a step of y = 2%), by fixing x (x = 2%)] were synthesized from high purity oxides: Pb_3O_4 (99.9 % M/S Aldrich chemicals, USA),TiO_2 (99.9% M/S s.d.fine-Chem Ltd.),

ZrO_2 (99.9 % M/S Aldrich chemicals, USA), Fe_2O_3 (99.9 % M/S Indian Rare-Earth Ltd), Sm_2O_3 (99.9 % M/S Aldrich chemicals, USA) and Nb_2O_5 (99.9 % M/S Aldrich chemicals, USA) using a high temperature solid-state reaction technique in an air atmosphere. The raw materials of the required compositions were mixed in a ball milling for 24 h in the presence of methanol using zirconia balls. The calcinations was done at a temperature 800 ^{O}C for 2h. Before compaction, the calcined lump was ground and granulated to convert it to a uniform free flowing aggregate by addition of small quantity of polyvinyl alcohol (PVA) as binder. The fine powder so obtained was pressed into discs (pellets) of 10 mm diameter and 1mm thickness under a pressure of 1000 kg cm^{-2} using a hydraulic press. The pellets were sintered in air atmosphere at 1150^{O}C for 2h in presence of $PbZrO_3$ powder, to prevent PbO loss during the high temperature sintering. Sintered pellets were electrode by high-purity silver particle paste, and fired at 750^{O}C, before using for any electrical measurements.

X-ray diffraction (XRD, Siemens D500) was used to determine the crystalline phases present in the powder. The compositions of the PZT phases were identified by the analysis of the peaks [(002)T, (200)R, (200)T] in the 2θ range 43˚ - 47˚. The tetragonal (T), rhombohedral (R) and tetragonal-rhombohedral phases were characterized and their lattice parameters were calculated. The rhombohedral lattice parameter was calculated on the assumption that the rhombohedral distortion was constant (unit cell angle α_R = 89.9˚) [14,15]. In order to ensure an accurate determination of the lattice parameters, the X-ray peaks were recorded gradually with 0.01˚ steps.

Densities of sintered pieces were calculated from the sample dimensions and weights. Microstructural features such as a grain size and pores were characterized by means of atomic force microscopy (AFM). The fractured surfaces were used for grain size and morphology determination. The size distribution of the grains was measured and the results compared with each other. The size distribution of the pores and the total value of porosity were determined on a polished cross-section of the samples with an image analyzer.

The dielectric response was measured at the frequency of 1 kHz by using an automatic LCR meter at a temperature ranging from a room temperature to 450˚C. Before measuring the piezoelectric properties, the specimens were poled in silicone oil at 110˚C by applying a d.c. field of 3.6 kV/mm for forty five minutes. Twenty four hours after poling, the piezoelectric properties: piezoelectric constant (d_{31}), electromechanical planar coupling factor (k_p) and mechanical quality factor (Q_m) were measured by a method similar to that of the IRE standard. The resonance and anti-resonance frequencies were obtained by using the maximum and the minimum of spectra admittance.

3. Results and discussion

3.1. Structural and morphology

Sintered powders were examined by X-ray diffractometry to ensure phase purity, and to identify the crystal structure. It can be seen that all the samples show pure perovskite structure, suggesting that Sm, Fe and Nb diffuse into the PZT lattice to form a solid solution. Fig.1 shows the XRD patterns of the sintered PZT–SFN samples with increasing Zr/Ti ratio. The content of the perovskite phase for all of the specimens is 100%. The tetragonal, rhombohedral and tetragonal–rhombohedral phases are identified by analysis of the peaks [002(tetragonal), 200(tetragonal), 200(rhombohedral)] in the 2θ range of 43°–47°. A transition from the tetragonal to the rhombohedral phase is observed as the Zr/Ti ratio increases. Firstly, incorporation of Fe^{3+} and Nb^{5+} in to B-sites of the perovskite structure for sample compositions near the MPB causes lattice variation, resulting in a small tolerance factor and stabilization of the rhombohedral phase compared with the tetragonal phase [16]. Secondly, increasing the Zr/Ti shifts the MPB region towards higher proportions of $PbZrO_3$. The compositions with $53 \leq y \leq 55$ were composed of a mixture of tetragonal and rhombohedral phases which are located near the MPB.

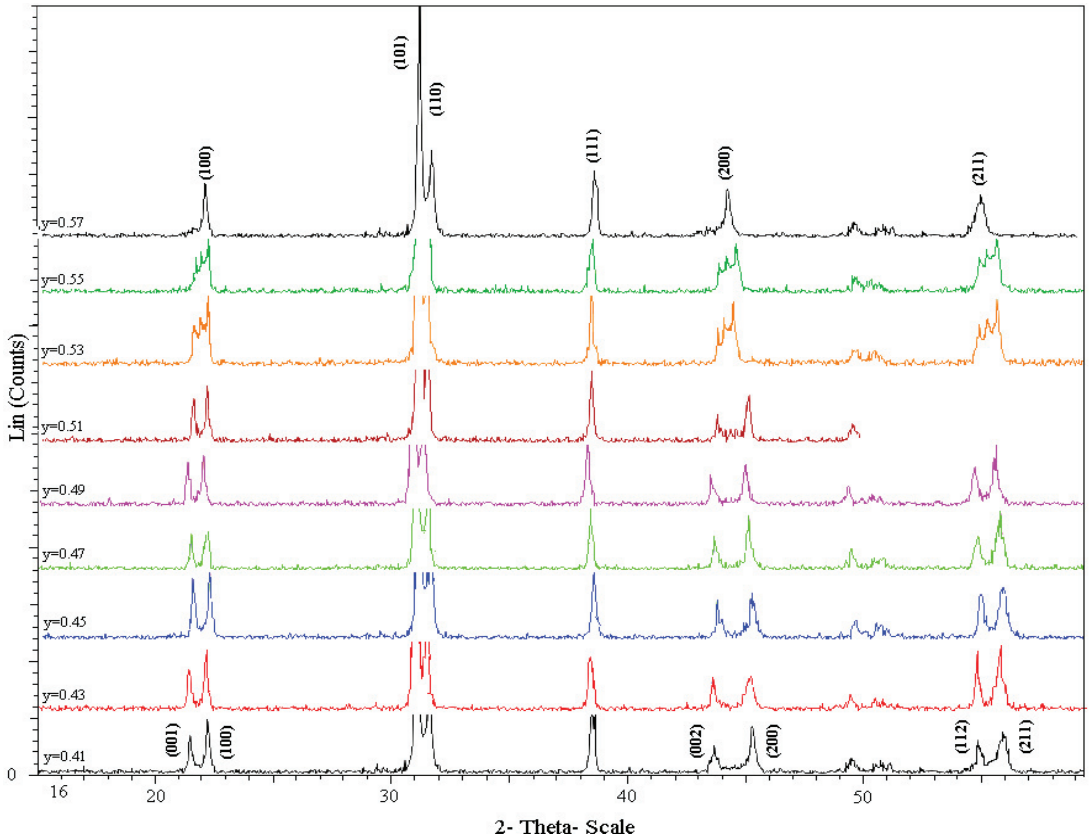

Fig. 1. XRD patterns of PZT–SFN ceramics sintered at 1150 °C for 2 h, with different Zr/Ti ratio.

Fig. 2(a)–(c) shows the surface morphologies of (1-x)Pb(Zr_y Ti_{1-y})O_3-xSm($Fe^{3+}_{0.5}$, $Nb^{5+}_{0.5}$)O_3 ceramics with y = 0.51, 0.53, and 0.55, respectively and the values of measured grain size are listed in Table 2. With the increase of Zr content, the (1-x)Pb(Zr_y Ti_{1-y})O_3-xSm($Fe^{3+}_{0.5}$, $Nb^{5+}_{0.5}$)O_3 ceramics become much denser, and their average grain size gradually increases, as shown in Fig.3. Huang et al [17], and Dixit et al [18] have reported that the morphology of Pb(Zr,Ti)O_3 materials is strongly dependent on the Zr content, and the Zr substitution helps improve the grain growth of these materials. The content of the rhombohedral phase gradually increases within creasing the Zr content [19], and thus the morphological evolution with Zr contents in present work may be attributed to the increase of a rhombohedral phase in these ceramics [18]. In order to further characterize the effect of Zr content on the density of all ceramics in this work, we measured their density, as shown in Fig.3. The density of the ceramics increases with increasing the Zr content from y =0–0.49, and then slightly increases with further increasing the Zr content for the ceramics with $0.51 \leq y \leq 0.55$. Therefore, the introduction of Zr plays an important role in the improvement of the density of PZT–SFN ceramics.

Table 2. The values grain size of PZT–SFN ceramics.

Zr content (mol%)	Grain size (μm)
51	1.88
53	2.50
55	2.15

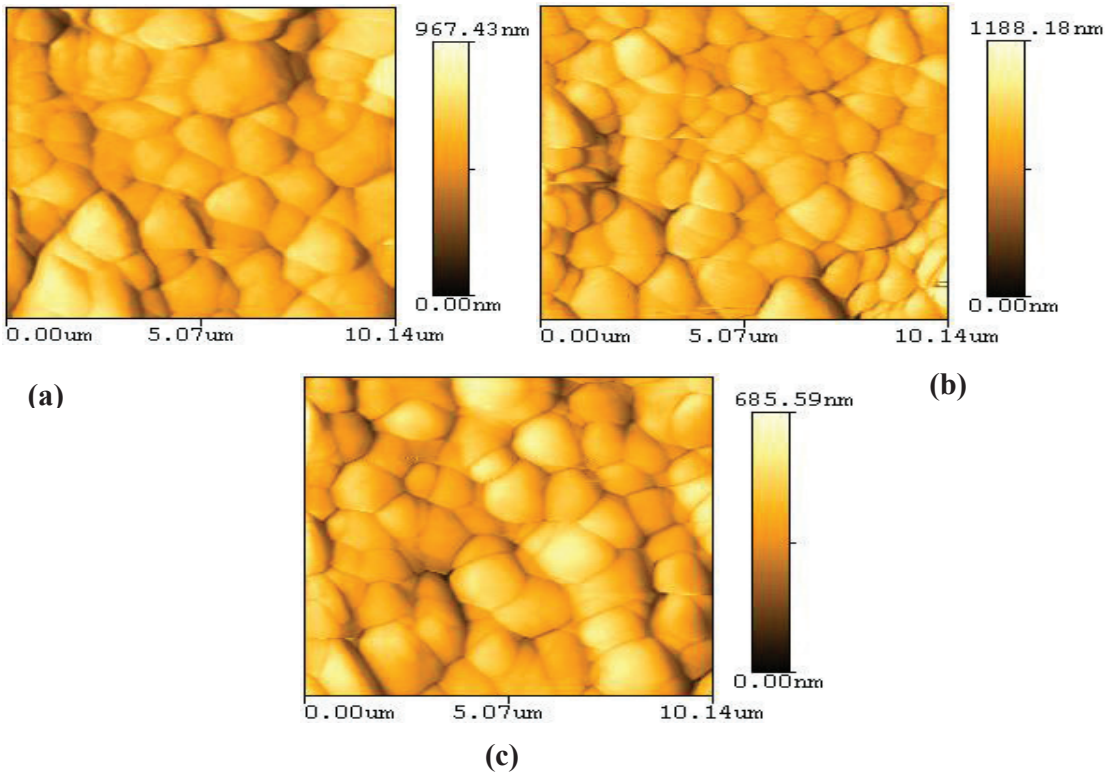

Fig. 2. AFM images of PZT-SFN ceramics sintered at 1150 °C for 2 h: (a) y=0.51, (b) y=0.53, and (c) y=0.55.

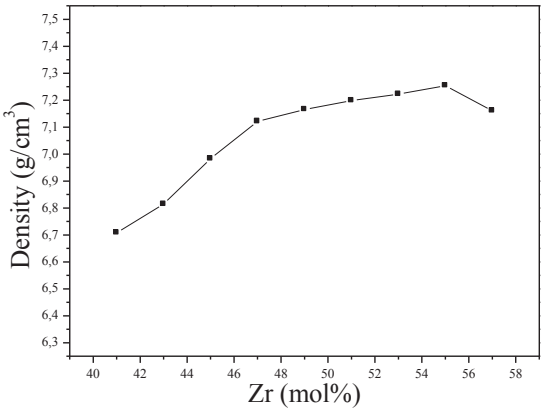

Fig. 3. Density according to the variation of Zr (mol%) in the composition of ceramics sintered at 1150 °C for 2 h.

3.2. Dielectric and piezoelectric properties

Dielectric measurement can give information about the electric properties of a material as a function of frequency and temperature. The analysis of dielectric property measures two electrical characteristics of the materials. One is capacitive which related to the insulating nature of the materials and it represents ability to store the charges and, second one is the conductive nature of the materials which gives the information about the electronic charge transport. Through this analysis, the dielectric constant (ε_r) and dielectric loss (tan δ) of a material can be determined which will explore the technological application. Plots of temperature variation of the dielectric constant (ε_r) measured at 1 kHz of the sample (1-x)Pb($Zr_y Ti_{1-y}$)O_3-xSm($Fe^{3+}_{0.5}$, $Nb^{5+}_{0.5}$)O_3 for y = 0.41-0.57 (sintered at 1150 ^{0}C) are shown in Fig. 4. The dielectric constant of the samples increases gradually with increasing temperature up to a temperature and thereafter it decreases. Dielectric constant increases with temperature due to interfacial polarization becoming more dominant compared to the dipolar polarization [20]. After a certain temperature reached, the dielectric constant decreases due to the phase transition from ferroelectric to paraelectric. The transition temperature is called Curie temperature (T_c) which was obtained from $|d\varepsilon_r/dT|$ versus temperature plot and those values are given in Table 3. We have observed that, the T_c decreases with the Zr concentration up to y = 0.55. Although we have observed increase of T_c for y = 0.57, but the value is almost comparable to that of y = 0.55. It is due to the decrease of lattice parameters, and bond lengths.

Table 3. Dielectric data of the sample (1-x)Pb($Zr_y Ti_{1-y}$)O_3-xSm($Fe^{3+}_{0.5}$, $Nb^{5+}_{0.5}$)O_3 for y = 0.41-0.57.

Zr content (mol%)	T_c (^{0}C)	ε_r
45	395	6807
47	390	9417
49	395	7554
51	385	9214
53	370	12499
55	370	12328
57	380	8033

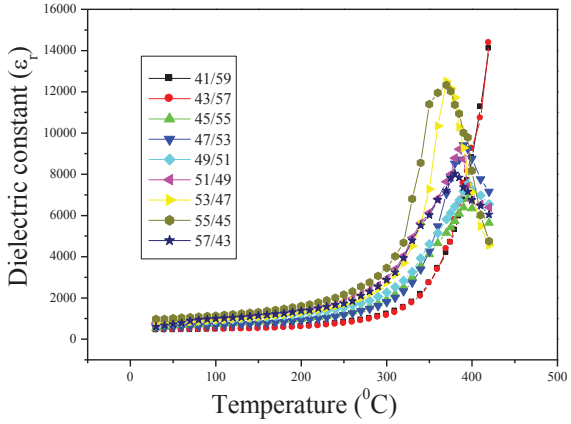

Fig. 4. Variation of dielectric constant of (1-x)Pb($Zr_y Ti_{1-y}$)O_3-xSm($Fe^{3+}_{0.5}$, $Nb^{5+}_{0.5}$)O_3 ceramics at 1 kHz as a function of temperature.

Fig.5 plots the temperature dependence of the dielectric loss (tgδ) behavior for the PZT–SFN ceramics, measured at 1 kHz. All the samples within the investigated temperature range (T ^{0}C = 30 -420) have dissipation factors <55%.

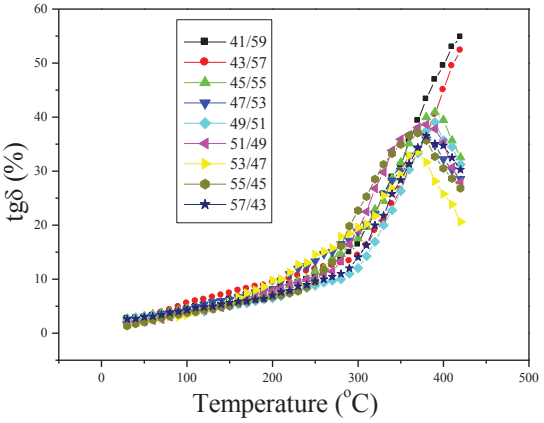

Fig. 5. Temperature dependence of dielectric loss (tgδ) for composite ceramics.

Plots of frequency versus dielectric constant for y = 0.41-0.57 are shown in Fig. 6(a). It is observed that, the dielectric constant decreases with frequency for all the samples. This can be explained in the fact that, at low frequencies ε_r is due to the contribution of multi component of polarizability, such as deformational (electronic and ionic) and relaxation (orientational and interfacial) polarizations. Electronic polarization arises from the displacement of the valence electrons relative to the positive nucleus. This type of polarization takes place up to the frequency 10^{16} Hz. Ionic type of polarization occurs due to the displacement of negative and positive ions with respect to each other. Maximum frequency of ionic polarization is 10^{13} Hz. Dipolar polarization occurs if the materials contain molecules with permanent electric dipole moment that can change orientation into the direction of the applied electric field. The dipolar polarization takes place at frequencies up to 10^{10} Hz. Space charge polarization occurs due to impedance mobile charge carriers by interfaces. It occurs at frequency range from 1 to 10^3 Hz. The

total polarization of the dielectric material can be explained as the sum of these 4 types of polarizations [21–23]. When the frequency is increased, the orientational polarization decreases since it takes more time than electronic and ionic polarizations. This decreases the value of relative dielectric constant ε_r reaching a constant value at higher frequency correspondingly to interfacial polarization. On the other hand the dielectric constant with temperature can be attributed to the fact that the orientational polarization is connected with thermal motion of molecules so dipole cannot orient themselves at low temperatures. When the temperature is increased the orientation of dipole is facilitated and this increases the orientational polarization which leads to increase of the dielectric constant with temperature. However after a certain temperature, the thermal energy is very high to restrict the polarization which leads to the disorder state (paraelectric). Hence, we have observed a transition from ferroelectric to paraelectric phase with the temperature.

The frequency dependence of dielectric loss (tanδ) of PZT–SFN is shown in Fig.6 (b). The dielectric loss decreases with frequency [24] and increases with temperature. This is a typical behaviour of ferroelectric materials. The nature of variation of tanδ at higher frequency and temperature can be explained by space-charge polarization [25].

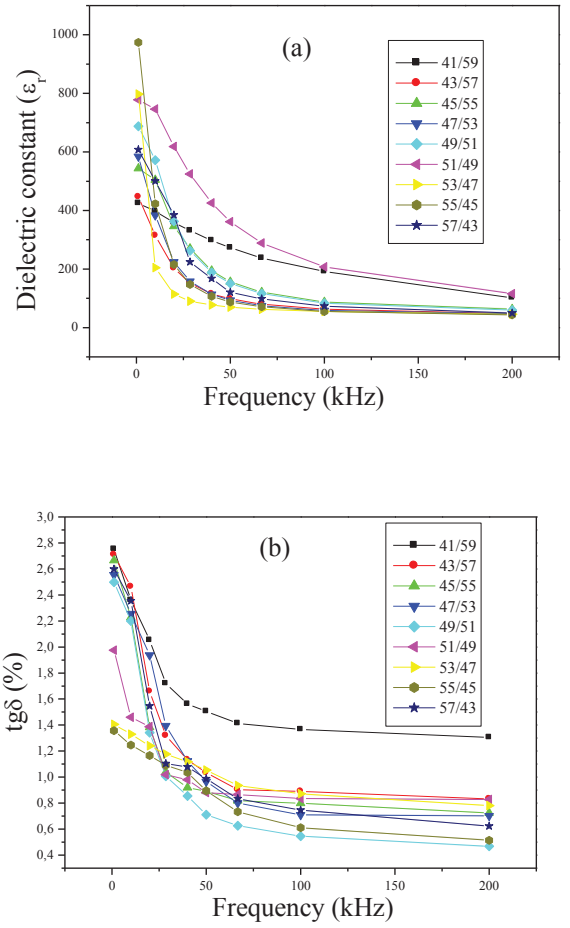

Fig. 6. Plots of frequency dependence on (a) dielectric constant and (b) dielectric loss of PZT–SFN ceramics measured at room temperature.

Fig. 7(a)–(b) shows d_{31}, g_{31}, K_p, and Q_m as a function of Zr content. PZT–SFN exhibits high d_{31}, g_{31} and K_p values around the MPB. The piezoelectricity achieves higher values around the MPB, while Q_m shows the opposite trend and is lower around the MPB. In the MPB region, the piezoelectricity reaches its maximum value due to piezoelectric interactions among the five existing domains, two of which belong to the tetragonal phase (180° and 90°) and three to the rhombohedral phase (180°, 71° and 109°). It can be seen that d_{31}>109.10^{-12} C/N, g_{31}>14.10^{-3} mV/N, K_p>0.61 and Q_m>92 around the MPB.

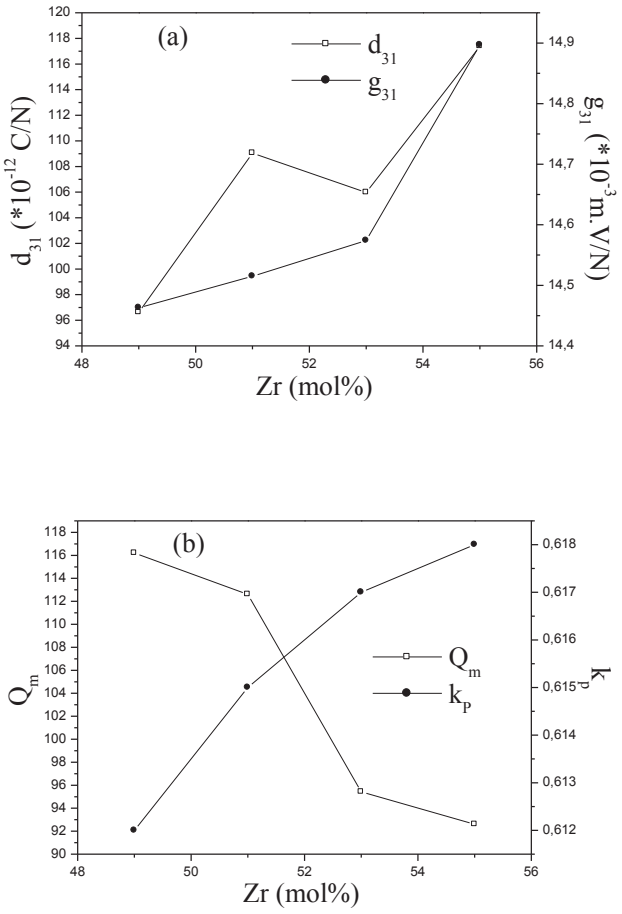

Fig. 7. (a-b) d_{31}, g_{31}, k_p, and Q_m of PZT–SFN as a function of Zr content.

4. Conclusion

These results reveal that the MPB of the tetragonal and rhombohedral phases coexist when PZT–SFN has a Zr composition of 0.53 ≤y≤ 0.55. The coexistence tetragonal and rhombohedral phases at 0.53 ≤y≤ 0.55 and the improvement in densification of the ceramics significantly enhance the piezoelectric and dielectric properties. The ceramics with y = 0.53-0.55 possess optimum properties: d_{31} =106-117 pC/N, g_{31} =14-15.10^{-3} m.V/N, K_p =61.7%-61.8% , Q_m =95-92, ε_r =798-974, tg δ =1.405%-1.356%, and T_c =370-370°C.

References

[1]Polla DL, Francis LF. M R S Bull 1996;21:59-65.
[2]Scott JF. Ferroelectric Memories. Springer: Berlin; 2000.
[3]Lin CT, Scanlan BW, Mcnell JD, Webb JS, Li L. J Mater Res 1992;7:2546-2554.
[4]Yokayama S, Ito Y, Ishihara H, Hamada K, Ohnishi S, Kudo J, Sakiyama K. Jpn J Appl Phys 1995;34:767-770.
[5]Neumann N, Kohler R, Hofmann G. Integrat Ferroelectric 1995;6:213-230.
[6]Haertling GH. J Am Ceram Soc 1999;82:797-818.
[7]Jaffe B, Cook WR. Piezoelectric Ceramics. RAN Publishers; 1971.
[8]Dai X, Xu Z, Viehland D. J Am Ceram Soc 1995;78:2815-2827.
[9]Jaffe B, Williams BC, Jaffe H. Piezoelectric Ceramics. Academic Press, London and New York; 1971.
[10]Yoshikawa Y, Tsuzuki K. J Am Ceram Soc 1992;75:2520-2528.
[11]Park SE, Shrout TR. J Am Ceram Soc 1997;80:1804-1811.
[12]Cross LE, Setter N, Colla EL. Ferroelectric Ceramics-Tutorial Review Theory, Processing and Applications, Birkhauser Verlag Basel 1993;1.
[13]Hardtl K, Henings D. J Am Ceram Soc 1972;55:230.
[14]Ari-Gur P, Benguigui L. Solid State Communications 1974;15:1077.
[15]Boutarfaia A, Bouaoud SE. Ceramics International 1996;22: 281-286.
[16]Yamashita Y, Hosono Y, Harada K, Ichinose N. Jpn J Appl Phys 2000;39:5593-5596.
[17]Dobal P, Dixit A, Katiyar R, Yu Z, Guo R, Bhalla A. Jpn J Appl Phy 2000;88:410-415.
[18]Dixit A, Majumder S, Dobal P, Katiyar R, Bhalla A. Thin Solid Films 2004;447:284-288.
[19]Huang H, Chiu H, Wu N, Wang M. Metall Mater Trans A 2008;39:3276-3284.
[20]Kittel C, Wiley J, Inc S. Introduction to Solid State Physics. New York/Singapore; 2006.
[21]Mahato DK, Choudhary RK, Srivastava SC. J Appl Sci 2006;93:716.
[22]Tang XG, Zhou QF, Zhang JX. J Appl Phys 1999;86:5194.
[23]Sahu N, Panigrahi S, Kar M. Ceramics International 2012;38:1549-1556.
[24]Shannigrahi SR, Tay FE H, Yao K, Choudhary RN P. J Europ Ceramic Soci 2004;24: 163.
[25]Lines ME, Glass AM. Principles and Applications of Ferroelectrics and Related Materials. Oxford University Press, London UK; 1977.